

Listen2Scene: Interactive material-aware binaural sound propagation for reconstructed 3D scenes

Anton Ratnarajah*

University of Maryland, College Park

Dinesh Manocha†

University of Maryland, College Park



Figure 1: We show the 3D reconstructed real-world environments with various levels of complexity that are used to evaluate our learning-based real-time sound propagation method and our audio rendering quality. In practice, our Listen2Scene approach is two orders of magnitude faster than the interactive geometric sound propagation algorithm. In our supplementary demo video, we show that the overall sound quality of Listen2Scene is very similar to the interactive geometric sound propagation algorithm.

ABSTRACT

We present an end-to-end binaural audio rendering approach (Listen2Scene) for virtual reality (VR) and augmented reality (AR) applications. We propose a novel neural-network-based binaural sound propagation method to generate acoustic effects for indoor 3D models of real environments. Any clean audio or dry audio can be convolved with the generated acoustic effects to render audio corresponding to the real environment. We propose a graph neural network that uses both the material and the topology information of the 3D scenes and generates a scene latent vector. Moreover, we use a conditional generative adversarial network (CGAN) to generate acoustic effects from the scene latent vector. Our network can handle holes or other artifacts in the reconstructed 3D mesh model. We present an efficient cost function for the generator network to incorporate spatial audio effects. Given the source and the listener position, our learning-based binaural sound propagation approach can generate an acoustic effect in 0.1 milliseconds on an NVIDIA GeForce RTX 2080 Ti GPU. We have evaluated the accuracy of our approach with binaural acoustic effects generated using an interactive geometric sound propagation algorithm and captured real acoustic effects / real-world recordings. We also performed a perceptual evaluation and observed that the audio rendered by our approach is more plausible than audio rendered using prior learning-based and geometric-based sound propagation algorithms. We quantitatively evaluated the accuracy of our approach using statistical acoustic parameters, and energy decay curves. The demo videos, code and dataset are available online ¹.

Index Terms: Computing methodologies—Machine learning—Machine learning approaches—Learning latent representations;

1 INTRODUCTION

Recent advances in computer vision and 3D reconstruction algorithms have made it possible to generate 3D models of real scenes in real-time [7, 8]. These reconstructed 3D models are used for ray-tracing simulation [61], surveying [55], visual analysis or interactive walkthroughs of buildings [25]. Furthermore, many tools or systems are available to transform real-life spaces into digital models [63], which offer higher visual fidelity than panoramic scans. The result-

ing static 3D models are used to generate immersive 3D experiences for VR or AR applications.

Many reconstructed models corresponding to apartments, houses, offices, public places, malls, or tourist attractions consist of multiple sound sources (e.g., human speaker, dishwasher, telephone, music). In order to improve the sense of the presence for a user, it is important to augment the visual realism with acoustic effects generated by these sources. It is well known that a user’s sense of presence in VR or AR environments can be improved by generating plausible sounds [22]. The resulting acoustic effects vary based on the location of each source, the listener and the environment characteristics [27]. In practice, the acoustic effects in VR or AR environments can be modeled using impulse responses (IRs), which capture how sound propagates from a source location to the position of the receiver in a given scene. IRs contain the necessary information for acoustic scene analysis such as the early reflections, late reverberation, arrival time, energy of direct and indirect sound, etc. The IR can be convolved with any dry sound (real or virtual) to apply the desired acoustic effects. Binaural IR characterizes the sound propagation from the sound source to the left and right ears of the listener. Unlike monaural IRs, binaural IRs have sufficient spatial information to locate the sound source accurately. Therefore binaural impulse responses (BIRs) give an immersive experience in AR and VR applications. It turns out that recording the BIRs in real scenes can be challenging and needs special capturing hardware. Furthermore, these BIRs need to be recaptured if the source or listener position changes.

In synthetic scenes, the IRs can be computed in real-time using sound propagation algorithms [27, 44]. However, current propagation algorithms are limited to synthetic scenes where an exact geometric representation of the scene and acoustic material properties are known a priori. On the other hand, generating a large number of high-quality IRs for complex 3D real scenes in real-time remains a challenging problem [6].

Recently, neural-network-based sound propagation methods to generate IRs have been proposed for interactive audio rendering applications [28, 39, 42, 54]. After training, the network can be used to generate a large number of IRs for 3D scenes. However, current learning methods have some limitations. They only deal with the mesh geometry, compute monaural IRs, and do not consider the acoustic material properties of the objects in the 3D scene. The material acoustic properties depend on the surface roughness, thickness and acoustic impedance [21, 51]. The materials in the 3D scene strongly influence the overall accuracy of the IR by controlling the amount of sound absorption and scattering when propagating sound waves interact with each surface in the scene. Moreover, current methods may not be directly applied to reconstructed 3D scenes

*e-mail: jeran@umd.edu

†e-mail: dmanocha@umd.edu

¹<https://anton-jeran.github.io/Listen2Scene/>

with significant holes.

Main Results: We present a novel neural-network-based sound propagation method to render audio for real indoor 3D scenes in real-time. Our approach is general and can generate BIRs for arbitrary topologies and material properties in the 3D scenes, based on the source and listener locations. Our sound propagation network comprises a graph neural network to encode the 3D scene materials and the topology, and a conditional generative adversarial network (CGAN) conditioned on the encoded 3D scene to generate the BIRs. The CGAN consists of a generator and a discriminator network. Some of the novel components of our work include:

1. Material-aware learning-based method: We represent the material’s acoustic properties using the frequency-dependent absorption and scattering coefficients. We calculate these material properties using average sound absorption and scattering coefficients for each vertex in a 3D scene from the input semantic labels of the 3D model and acoustic material databases. We propose an efficient approach to incorporate material properties in our Listen2Scene architecture. Our method results in 48% better accuracy over prior learning methods in terms of acoustic characteristics of the IRs.

2. Binaural Impulse Response (BIR) Generation: We present a simple and efficient cost function to the generator network in our CGAN to incorporate spatial acoustic effects such as the difference in the time-of-arrival of sound arriving in left and right ears (interaural time difference) [62] and sound level difference in both ears caused by the barrier created by the head when the sound is arriving (interaural level difference).

3. Perceptual evaluation: We performed a user study to evaluate the benefits of our proposed audio rendering approach. We rendered audio for 5 real environments with different levels of complexity with the number of vertices in the selected environments varying from 0.5 million to 2.5 million (Fig. 1) and asked the participants to choose between our proposed approach and the baseline methods. More than 67% and 45% of the participants observed that the audio rendered from Listen2Scene is more plausible than the prior learning-based approach MESH2IR and interactive geometric-based sound propagation algorithm respectively. We also compared the audio rendering using our approach with recorded IRs [3] where the materials are an independent variable.

4. Novel Dataset: We generate 1 million high-quality BIRs using the geometric-based sound propagation method [48] for around 1500 3D real scenes in the ScanNet dataset [7]. Among 1 million BIRs, we randomly sampled 200,000 BIRs to train our network. We release the full BIR dataset in the wav format ².

We have evaluated the accuracy of our approach using the captured BIRs from the BRAS dataset [3] and synthetic BIRs generated using the geometric propagation approach for real scenes not used during training. Our network is capable of generating 10,000 BIRs per second for a given 3D scene on an NVIDIA GeForce RTX 2080 Ti GPU. In practice, we observe two orders of magnitude performance improvement over interactive sound propagation algorithms.

2 RELATED WORKS

Sound Propagation and IR Computation: The IRs can be computed using wave-based [1, 14, 31, 60] or geometric [23, 47, 49] sound propagation algorithms. The wave-based algorithms are computationally expensive, and their runtime is proportional to the third or fourth power of the highest simulation frequency [36]. For interactive applications, IRs are precomputed for a 3D scene grid and IRs are calculated at run time for different listener positions

²https://drive.usercontent.google.com/download?id=1FnBadVRQvtV9jMrCz_F-U_YwjvxxK8s0&authuser=0

using efficient interpolation techniques [30, 37]. Geometric sound propagation algorithms are based on ray tracing or its variants and can be used for interactive applications [6, 48]. They can handle dynamic scenes and work well for high frequencies. Many hybrid combinations of geometric and wave-based methods have been proposed [59]. These methods are increasingly used for games and VR applications and can take tens of milliseconds to compute each IR on commodity hardware.

Learning-based sound propagation: Learning-based sound propagation methods for IR computation have been proposed to generate IRs based on a single image of the environment [19, 29, 52], reverberant speech signal [38, 53], or shoe-box shaped room geometry [42]. Neural networks are also used to translate synthetic IRs to real IRs and to augment IRs [40, 41] and estimate room acoustic parameters [10, 13, 45]. Learning-based approaches are proposed to learn the implicit representation of IRs for a given 3D scene and predict IRs for new locations on the same training scene [28, 54]. MESH2IR [39] is a sound propagation network that takes the complete 3D mesh of a 3D scene and the source and the listener positions as input and generates monaural IRs in real-time on a high-end GPU. However, the audio rendered using these learning-based sound propagation methods may not be smooth and can have artifacts. Prior learning-based binaural sound propagation methods require a few BIRs captured in a new 3D scene to generate new BIRs for different source and listener locations in the same 3D scene [29]. Our learning-based sound propagation method is more accurate and general than prior methods.

Real Scenes. The materials in the real scene influence the acoustic effects corresponding to the scene. The material information can be estimated from images and videos of real scenes and given as input to sound propagation algorithms using material acoustic coefficients [5, 46, 58]. Other methods are based on capturing reference audio samples or IRs in real scenes and the simulated IRs are adjusted to match the materials using reference audios or IRs [24, 43, 57]. In recent works, real scenes are annotated using crowd-sourcing [7] and material acoustic coefficients can be estimated by mapping the real scenes’ annotated material labels to materials in the existing acoustic coefficient database [6, 56]. As compared to these methods, our approach is either significantly faster or generates higher-quality acoustic effects in real scenes.

3 MODEL REPRESENTATION AND DATASET GENERATION

Our approach is designed for real scenes. We use 3D reconstructed scenes from the RGB-D data captured using commodity devices (e.g., iPad and Microsoft Kinect). These reconstructed 3D scenes are segmented and the objects in the 3D scene can be annotated by crowdsourcing [7, 8]. Our goal is to use these mesh representations and semantic information to generate plausible acoustic effects. An overview of our approach is given in Fig. 2.

We preprocess the annotated 3D scene to close the holes in the reconstructed 3D scene and simplify the 3D scene by reducing the number of faces. We perform mesh simplification using graph processing to reduce the complexity of the 3D scene input into our network. We represent the simplified 3D scene as a graph GN and input GN to our graph neural network Net_{GR} (Fig. 4) to encode the input 3D scene as an 8-dimensional latent vector. Then we pass the encoded 3D scene latent vector along with the listener position LP and the source position SP to our generator network Net_{GN} (Fig. 2) to generate binaural impulse response BIR (Equation 1).

$$BIR = Net_{GN}(Net_{GR}(GN), LP, SP). \quad (1)$$

We rendered audio S_R for the given spatial locations of the receiver and listener in a given 3D scene at time t by convolving the

corresponding *BIR* with any clean or dry audio signal S_C (Equation 2).

$$S_R[t] = S_C[t] \otimes BIR[t]. \quad (2)$$

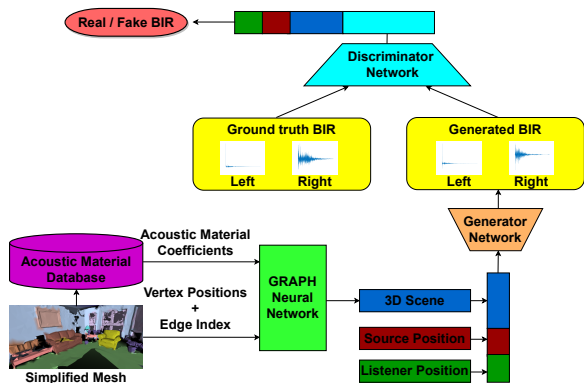


Figure 2: The overall sound propagation architecture of our Listen2Scene method: The simplified 3D scene mesh with material annotations is passed to the acoustic material database to estimate the acoustic material coefficients (absorption and scattering coefficient). We pass the acoustic material coefficients, vertex positions, and edge index to our graph neural network (Fig. 4) to encode the 3D scene into a latent vector. Our generator network takes the 3D Scene and listener and source positions as input and generates a corresponding BIR. The discriminator network discriminates between the generated BIR and the ground truth BIR during training.

3.1 Dataset Creation

There aren't real-world and synthetic BIR datasets for a wide range of real 3D scenes captured using commodity hardware available to train our Listen2Scene. Therefore we create synthetic BIRs using a geometric simulator [58] for 3D reconstructed real-world scenes in the ScanNet dataset [7] to train our Listen2Scene. We preprocess the 3D meshes and assign meaningful acoustic material properties to each object and surface in the 3D scene (§ 3.1.1). Next, we sample source and listener positions and simulate BIRs using the geometric simulator (§ 3.1.2).

3.1.1 Mesh Preprocessing and Material Assignment

The ScanNet dataset contains vertex-level segmented mesh. To make the dataset compatible with a geometric-based sound propagation system, we convert vertex-level segmentation of the 3D scene to face-level segmentation of the 3D scene. Face-level segmentation is used to assign material acoustic coefficients to each surface in the 3D scene. Many of the meshes in the ScanNet dataset have holes in the surface boundary and the ceiling is not present. The holes can prevent some of the sound rays from reflecting back to the listener and result in generating unrealistic acoustic effects using the ray tracing-based geometric sound propagation algorithm. We compute the convex hull of the overall 3D scene mesh and merge it with the original mesh to close the holes in the outer surface boundaries. We fill small holes on internally separated spaces using fill_holes() function in the trimesh library [9].

The ScanNet dataset also contains the semantic annotation (i.e., instance-level object category labels such as dish rack, wall, laundry basket etc.) for every 3D scene. We use the absorption coefficient acoustic database with more than 2000 materials [17] to get the absorption coefficient of each material in the ScanNet 3D reconstructions. We do not always find exact ScanNet object labels in the acoustic database. Therefore, we use the natural language processing (NLP) technique to find the closest matching material in the acoustic database for every ScanNet object label and assign its

absorption coefficient to the ScanNet object label. To find the closest matching material, we encode the object labels in ScanNet and material names in the acoustic database into fixed-length sentence embeddings [33]. Transformer-based sentence embedding vectors are close in cosine similarity distance for sentences with similar meaning and outperform in many NLP tasks [26]. We use the Microsoft pre-trained sentence transformer model to encode materials into 768-dimensional sentence embedding. We use the cosine similarity of the ScanNet object labels and materials in the acoustic database and assign the closest materials absorption coefficients to the objects in the ScanNet.

In addition to absorption coefficients, we need scattering coefficients for geometric sound propagation. The scattering coefficients are not available in the acoustic database [17]. Therefore, we adapt the sampling approach proposed in GWA [56]. We fit a Gaussian distribution by calculating the mean and standard deviation of 37 sets of scattering coefficients collected from the BRAS benchmark [3] and we sample randomly from the distribution for every 3D scene.

3.1.2 Geometric Sound Propagation

For every 3D scene, we perform grid sampling with 1m spacing in all three dimensions. We also ensure that there is a minimum gap of 0.2 m between the sampled position and objects in the scene to prevent collisions. The number of grid samples varies with the dimension of the 3D scene. We randomly place 10 sources in the grid sampled locations and the rest of the samples are assigned to listener locations. We perform geometric simulations for every combination of listener and source positions. We use 20,000 rays for geometric propagation and the simulation stops when the maximum depth of specular or diffuse reflection is 2000 or the ray energy is below the hearing threshold.

4 OUR LEARNING APPROACH

In this section, we present the details of our learning method. Our approach learns to generate BIRs for 3D reconstructed real scenes, which may have noise or holes. We first present our approach to representing the topology and material details of the 3D scene using our graph neural network (§ 4.1). Next, we present our overall architecture, which takes the 3D scene and generates plausible BIRs and training details (§ 4.2).

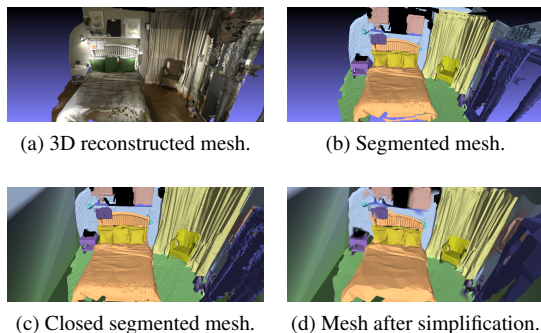


Figure 3: The 3D reconstruction of the real scene from the ScanNet (a); object category-level segmentation of the 3D scene with each category is represented by a different color (b); the modified mesh after closing the holes using convex hull (c); the simplified mesh with object-level segmentation information preserved (d); we observe that high-level object shapes (e.g., bed, office chair, wooden table, etc.) and materials are preserved even after simplifying the mesh to 2.5% of the original size.

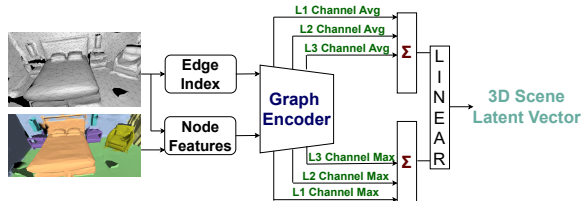


Figure 4: Our network architecture represents a 3D scene as an 8-dimensional latent vector. The vertex positions and material properties are combined to produce the node features. We pass the edge index and node features from the 3D scene as input to the graph encoder. The graph encoder consists of 3 graph layers (L1, L2, and L3). The channel-wise average and the channel-wise maximum of the node features in each layer are aggregated and passed to linear layers. Linear layers output a 3D scene latent vector.

4.1 3D Scene Representation

The ScanNet dataset represents the RGB-D data collected from the 3D scene in the form of a 3D mesh. The shapes of the objects in the 3D scene are represented using the vertices and triangular faces in the 3D Cartesian coordinates. The ScanNet dataset also provides object category labels at the vertex level. We perform the mesh preprocessing and material assignment approach as mentioned in § 3.1.1. To reduce the size and complexity of the data passed to the neural network while preserving high-level object details, we adapt and modify prior work [39] by performing mesh simplifications using PyMeshlab’s implementation of the quadratic-based edge collapse mesh simplification algorithm [34]. We simplify the meshes to have only 2.5% of the initial number of faces. The mesh simplification algorithm can simplify the mesh while preserving the vertex-level segmentation of the mesh (Fig. 3). The simplified meshes typically have around 10,000 faces.

In Fig. 3, we observe that segmented mesh interpolates the nearby materials to the closed holes (e.g., holes near the floor are assigned to materials of the floor and the material is represented in green). We observe that even after mesh simplification to 2.5% of the original size, high-level object structures are preserved.

The triangular mesh of the 3D scene can be represented using graph $G = \langle V, E \rangle$, where V represents the 3D Cartesian coordinates of the set of vertices/nodes and E is the connectivity of each node (edge index). The vertex coordinates of three dimensions are features of the node in a graph. To add the material properties of the 3D scene, we increase the node feature dimension to five. The material properties can be represented using the material’s absorption coefficient and scattering coefficient. The absorption coefficient represents how much sound can be absorbed by the material. Metal absorbs the least sound and has a very low coefficient. A cushion is a sound-absorbing material and has a high coefficient. The scattering coefficient represents the roughness of the material’s surface. When the surface is rough, the sound will be scattered in all directions and has a high coefficient; smooth surfaces have a low coefficient value. The absorbing and scattering coefficients are frequency-dependent coefficients. The coefficients are defined for the 8-octave bands between 62.5 Hz and 8000 Hz. To reduce the dimensionality of the coefficients, we calculate the average coefficients by taking the coefficients at 500 Hz and 1000 Hz. We show the benefit of our approach of calculating average coefficients at 500 Hz and 1000 Hz in § 6.2. In many practical applications, the average value of room acoustics parameters like reverberation time is used for analysis instead of all the values at different octave bands [6, 41, 57]. We increase the node features V by combining (x, y, z) Cartesian coordinates of the vertex with the average absorption coefficient ab and average scattering coefficient sc ($V = [x, y, z, ab, sc]$).

We input node features and edge index to the graph encoder

network to encode the 3D scene to a low dimensional space. The encoder network has 3 layers. In each layer, the graph convolution layer [16] is used to encode the node features (Equation 3). We gradually reduce the size of the graph by dropping the number of node features to 0.6 times the original number of node features in each layer using the graph pooling layer.

In Equation 3, the adjacency matrix representing the edge index of the 3D scene (A) and the identity matrix I are aggregated to calculate \hat{A} ($\hat{A} = A + I$). Each column of \hat{A} is summed to get diagonal matrix \hat{D} ($\hat{D}_{ii} = \sum_j \hat{A}_{ij}$). $W^{(n)}$ is a trainable weight matrix for layer n . Node features at layers n and $n + 1$ are $N_F^{(n)}$ and $N_F^{(n+1)}$, respectively.

$$N_F^{(n+1)} = \sigma(\hat{D}^{-\frac{1}{2}} \hat{A} \hat{D}^{-\frac{1}{2}} N_F^{(n)} W^{(n)}), \quad (3)$$

The output of the graph convolution layer is passed to the graph pooling layers [11, 18] to simplify the graph by reducing the node features and edge index. The graph pooling layer initially calculates the square of the adjacency matrix ($A_{new}^{(n)} = A^{(n)} A^{(n)}$) to increase the graph connectivity and is used to choose the top N node features. The adjacency matrix $A_{new}^{(n)}$ prevents isolated edges in the graph encoded 3D scene when choosing top N node features from the input graph and discarding other features.

We calculate the channel-wise average and channel-wise maximum of the output node features in each graph layer in the graph encoder network. We aggregate the channel-wise average and channel-wise maximum separately over the 3 layers. We concatenate the aggregated maximum and aggregated average values and pass them as input to a set of linear layers. We concatenate the learned features in each layer to ensure that the linear layers use all the learned features to construct an accurate 3D scene latent vector of dimension 8 as an output from the linear layer.

4.2 BIR Generation

We use a one-dimensional modified conditional generative adversarial network (CGAN) to generate BIRs. The standard CGAN architectures [12, 32] generate multiple different samples corresponding to input condition y by changing the input random noise vector z . In our CGAN architecture, we only input the condition y to generate a single precise output. Our CGAN network takes a 3D scene latent vector as the input condition and generates a single precise BIR. We propose a novel cost function to trigger the network to generate binaural effects such as interaural level difference (ILD) and interaural time difference (ITD) accurately.

We extend the IR preprocessing approach proposed in MESH2IR to make the network learn to generate BIRs with large variations of standard deviation (SD) efficiently. In § 3.1, we generate high-fidelity BIRs with a sampling rate of 48,000 Hz. We initially down-sample the BIRs to 16,000 Hz to represent a longer duration of BIRs. We train our network to generate around 0.25 seconds (3968 samples) of BIR to reduce the complexity of the network. Our architecture can be easily modified to train the network to generate any duration of BIRs. The complexity of our network changes linearly with the duration of generated BIRs. We calculate the SD of the BIR and divide the BIR with SD to have fewer variations over training samples. We replicate the SD 128 times and concatenate it towards the end of the BIR. Therefore, each channel of the preprocessed BIR will have 4096 samples (3968+128). We train our network to generate preprocessed BIRs. Later, we can recover the original BIR by removing SD represented in the last 128 samples, getting the average of SD values, and multiplying the first 3968 samples by the average SD value. We get the average SD over 128 samples to reduce the error of the recovered SD.

Our CGAN architecture consists of a generator network (G) and a discriminator network (D) (Fig. 2). We pass the 3D scene information Γ_S consisting of mesh topology and materials of the 3D scenes represented using a latent vector, and the listener and source position

as an input to G . We train the G and the D in our CGAN architecture using our created BIRs (§ 3.1) and Γ_S in the data distribution p_{data} . We train G to minimize the objective function \mathcal{L}_G and the D to maximize the objective function \mathcal{L}_D alternately.

Generator Objective Function (\mathcal{L}_G): The \mathcal{L}_G is minimized during training to generate accurate BIRs for the given condition Γ_S . The \mathcal{L}_G (Equation 4) consists of modified CGAN error (\mathcal{L}_{CGAN}), BIR error (\mathcal{L}_{BIR}), ED error (\mathcal{L}_{ED}), and mean square error (\mathcal{L}_{MSE}). The contribution of each individual error is controlled using the weights λ_{BIR} , λ_{ED} and λ_{MSE} :

$$\mathcal{L}_G = \mathcal{L}_{CGAN} + \lambda_{BIR} \mathcal{L}_{BIR} + \lambda_{ED} \mathcal{L}_{ED} + \lambda_{MSE} \mathcal{L}_{MSE}. \quad (4)$$

The modified CGAN error is minimized when the BIRs generated using G are difficult to differentiate from the ground truth BIRs by D for each 3D scene Γ_S :

$$\mathcal{L}_{CGAN} = \mathbb{E}_{\Gamma_S \sim p_{data}} [\log(1 - D(G(\Gamma_S), \Gamma_S))]. \quad (5)$$

The time of arrival of the direct signal and the magnitude levels of the left and right channels of the BIRs vary significantly with the direction of the sound source. To make sure the network captures the relative variation of the IRs in the left and right channels, we propose the BIR error formulation.

$$\mathcal{L}_{BIR} = \mathbb{E}_{(B_G, \Gamma_S) \sim p_{data}} [\mathbb{E}_{c \sim c} [((B_{LN}(\Gamma_S, s) - B_{RN}(\Gamma_S, s)) - (B_{LG}(\Gamma_S, s) - B_{RG}(\Gamma_S, s)))^2]], \quad (6)$$

where B_{LN} and B_{RN} are the left and right channels of the BIRs generated using our network and B_{LG} and B_{RG} are the left and right channels of the ground truth BIRs.

The energy remaining in the BIR (b) with respect to the time t_i seconds and at frequency band with center frequency f_c Hz (Equation 7) is described using energy decay relief (ED) [15, 50]. In Equation 7, the bin c of the short-time Fourier transform of b at time t is defined as $H(b, t, c)$. The ED curves decay smoothly over time and they can be converted into an "equivalent IR" [20]. In previous works [38, 39], it is observed that ED helps the model to converge.

$$ED(b, t_i, f_c) = \sum_{c=1}^T |H(b, t, c)|^2. \quad (7)$$

The ED curves reduce exponentially over time. In previous works [39], the mean square error (MSE) between the ED curves of the ground truth BIR (B_G) and the generated BIR (B_N) is calculated. This approach does not capture the latter part of ED curves accurately. Therefore we compare the log of the ED curves between ground truth and generated BIRs for each sample (s) as follows:

$$\mathcal{L}_{ED} = \mathbb{E}_{(B_G, \Gamma_S) \sim p_{data}} [\mathbb{E}_{c \sim c} [\mathbb{E}_{s \sim s} [(\log(ED(B_G(\Gamma_S), c, s)) - \log(ED(B_N(\Gamma_S), c, s)))^2]]. \quad (8)$$

To capture the structures of the BIR, we also calculate MSE error in the time domain. For each 3D scene Γ_S we compare B_G and B_N over the samples (s) of BIR as follows:

$$\mathcal{L}_{MSE} = \mathbb{E}_{(B_G, \Gamma_S) \sim p_{data}} [\mathbb{E}_{s \sim s} [(B_G(\Gamma_S, s) - B_N(\Gamma_S, s))^2]]. \quad (9)$$

Discriminator Objective Function (\mathcal{L}_D): The discriminator (D) is trained to maximize the objective function \mathcal{L}_D (Equation 10) to differentiate the ground truth BIR (B_G) and the BIR generated using the generator (G) during training for each 3D scene Γ_S .

$$\mathcal{L}_D = \mathbb{E}_{(B_G, \Gamma_S) \sim p_{data}} [\log(D(B_G(\Gamma_S), \Gamma_S))] + \mathbb{E}_{\Gamma_S \sim p_{data}} [\log(1 - D(G(\Gamma_S), \Gamma_S))]. \quad (10)$$

Network Architecture and Training: We extend the standard time domain Generator (G) and Discriminator (D) architectures proposed for monaural IR generation [39, 42]. We modify G to take our 3D scene latent vector of 8 dimensions (Fig. 4) and the source and listener positions in 3D Cartesian coordinates. Our G takes 14-dimensional conditional vectors and generates 4096x2 preprocessed BIR as output. We also modify our D to differentiate between two

channel ground truth and generated BIRs. We train all networks with a batch size of 96 using an RMSprop optimizer. The hyperparameter is chosen manually by looking at how the network converges at the initial epochs. We initially started with a learning rate of 8×10^{-5} , and the learning rate decayed to 0.7 of its previous value every 7 epochs. We trained our network for 100 epochs.

5 ABLATION EXPERIMENTS

We perform ablation experiments to analyze the contribution of our proposed BIR error (Equation 6) and Energy Decay (ED) error (Equation 8) in training our network. We also analyze the performance of the network with and without closing holes in the 3D mesh. We generated 900 BIRs for 20 real testing environments for our ablation study.

5.1 BIR Error

Our BIR error (Equation 6) helps to generate binaural acoustic effects by incorporating magnitude level differences between the left and right channels of BIRs. In Fig. 5, we plot the difference between the left and right channels of the ED curve of BIRs generated using a geometric-based approach, Listen2Scene and Listen2Scene approach trained without BIR error (Listen2Scene-No-BIR). We can observe that incorporating BIR error reduces the gap between the geometric approach (ground truth) and our Listen2Scene.

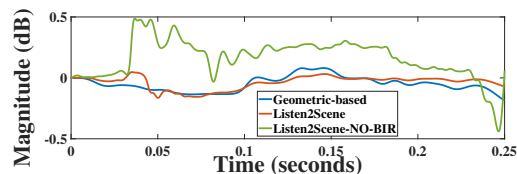


Figure 5: The normalized difference in energy decay (ED) curves of left and right channels of BIR. The BIRs are generated using the geometric method, Listen2Scene and Listen2Scene-No-BIR (Listen2Scene trained without BIR error). We observe that the ED curve difference of Listen2Scene closely matches the geometric method.

5.2 ED Error

We trained our Listen2Scene network with the ED error proposed in MESH2IR [39] (Listen2Scene-ED) and our proposed ED error (Equation 8). We calculated the MSE between the normalized ED curves of the ground truth BIRs from the geometric-based approach and the generated BIRs over the center frequencies 125Hz, 500Hz, 1000Hz, 2000Hz and 4000 Hz covering voice frequency and reported in Table 1. We can see that MSE of the normalized ED curves in the testing environment is low for our proposed ED error (Listen2Scene). Fig. 6, shows the normalized ED curves of the left channel BIR from the geometric-based method, Listen2Scene and Listen2Scene-ED at 2000Hz. We can see that the ED curve of Listen2Scene-ED diverges from the geometric-based method after 0.1 seconds.

5.3 Closed and Open Mesh Models

We trained and evaluated our Listen2Scene network using the default 3D mesh with holes (Listen2Scene-Hole) and a closed mesh using our proposed approach (§ 3.1.1). We can see in Table 2 that the BIRs generated using Listen2Scene match the geometric-based sound propagation algorithm. Fig. 7, shows the left channel of the BIR from the geometric-based approach and the corresponding BIR from Listen2Scene-Hole. We can see that the BIRs from the geometric-based approach and Listen2Scene-Hole are significantly different.

Table 1: The MSE error between the normalized energy decay (ED) curves of the ground truth BIRs from the geometric sound propagation algorithm and the generated BIRs from our Listen2Scene and Listen2Scene trained with ED error proposed in MESH2IR [39] (Listen2Scene-ED). We calculate the MSE over the center frequencies 125Hz, 500Hz, 1000Hz, 2000Hz and 4000 Hz. The best results are shown in **bold**

Method	Frequency				
	125Hz	500Hz	1000Hz	2000Hz	4000Hz
Listen2Scene-ED	2.58	3.28	3.99	4.16	4.23
Listen2Scene	2.50	2.93	3.54	3.56	3.56

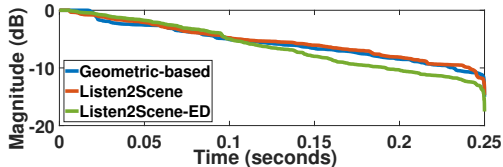


Figure 6: The normalized energy decay (ED) curve of the BIRs (left channel) generated using the geometric-based method, Listen2Scene and Listen2Scene-ED (Listen2Scene trained with ED error proposed in MESH2IR [39]) at 2000 Hz. We can see that the ED curve of Listen2Scene matches the geometric method for the entire duration while the ED curve of Listen2Scene-ED starts diverging after 0.1 seconds.

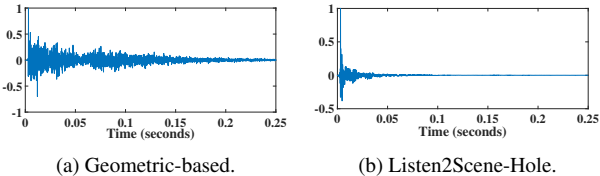


Figure 7: The left channel of the BIR generated using a geometric-based sound propagation algorithm and our Listen2Scene approach without closing the holes (Listen2Scene-Hole). We can see that the BIR from Listen2Scene-Hole significantly varies from the geometric-based approach.

6 ACOUSTIC EVALUATION

6.1 BRAS Benchmark

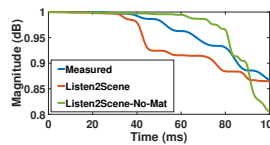
We use the BRAS benchmark [3] to evaluate the contribution of material properties to the accuracy of the BIR generated using our Listen2Scene method. The BRAS contains a complete scene description, including the captured BIRs (i.e. ground truth) and the 3D models with semantic annotations for a wide range of scenes. We trained our approach without including the material properties (Listen2Scene-No-Mat) and including material properties (Listen2Scene). We evaluate our approach using recorded BIRs from the chamber music hall and auditorium (Fig. 8). We generated BIRs corresponding to the source and listener positions in the same 3D models and compared the accuracy. We plot the normalized early reflection energy decay curves (EDC) of the captured BIRs and the BIRs generated using our models (Fig. 8). The EDC describes the amount of energy remaining in the BIR with respect to time [50]. We observe that in 2 different scenarios, adding material improves the energy decay pattern of the BIRs. We calculated the mean absolute error (MAE) between the EDC of captured BIRs and generated BIRs. MAE decreases by 3.6% for the medium room and 6.6% for the large room.



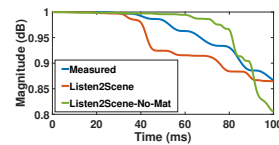
(a) Chamber music hall (Medium).



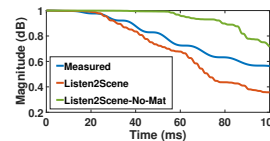
(b) Auditorium (Large).



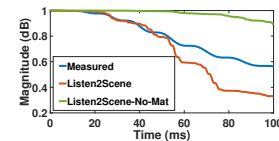
(c) Left channel.



(d) Right channel.



(e) Left channel.



(f) Right channel.

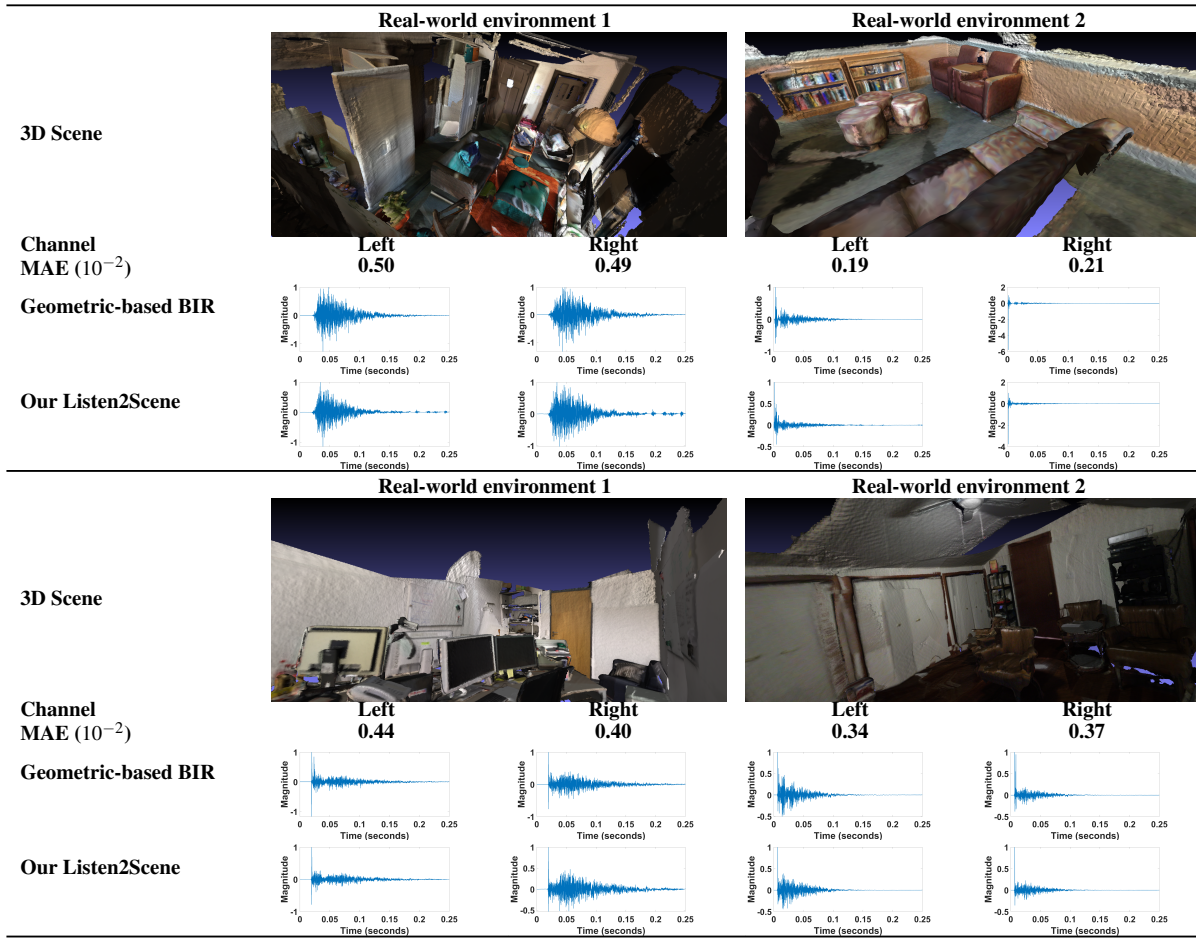
Figure 8: The normalized energy decay curves (EDC) of the captured BIRs and the BIRs generated using our approach with material (Listen2Scene) and without material (Listen2Scene-No-Mat) for the 3D scenes in BRAS ((a),(b)). We plot the EDC for the BIRs from the chamber music hall ((c),(d)) and auditorium ((e),(f)). We observe that the EDC of Listen2Scene is closer to the EDC of captured BIRs.

6.2 Accuracy Analysis

We quantitatively evaluate the accuracy of our proposed approach using standard acoustic metrics such as reverberation time (T_{60}), direct-to-reverberant ratio (DRR), and early-decay-time (EDT). T_{60} measures the time taken for the sound pressure to decay by 60 decibels (dB). The ratio of the sound pressure level of the direct sound to the sound arriving after surface reflections is DRR [35]. The six times the time taken for the sound pressure to decay by 10 dB corresponds to EDT. We generate 2000 high-quality BIRs using many rays with the geometric method [48] for 166 real scenes not used to train our networks in the ScanNet dataset. We compare the accuracy of Listen2Scene with the BIRs computed using the geometric method on these scenes.

In our Listen2Scene network, we pass the average sound absorption and reflection coefficients at 500 Hz and 1000 Hz as input. In our Listen2Scene-Full variant, the average coefficient over the 8-octave bands between 62.5 Hz and 8000 Hz is given as input. Also, in our Listen2Scene, we simplify the mesh to 2.5% of the original size. Our Listen2Scene-Fix variant simplifies all the meshes to have a constant number of faces (2000 faces). The motivation behind our approach is that we empirically observed that instead of having a fixed size if we simplify the meshes to 2.5% of the original size, the contextual information is preserved better. We calculate the mean absolute acoustic metrics error of the BIRs generated using our approach with materials (Listen2Scene) and without materials (Listen2Scene-No-Mat), Listen2Scene-ED, Listen2Scene-No-BIR, Listen2Scene-Fix and Listen2Scene-Full. We report the average error from two channels in our generated BIRs (Table 4). Many prior learning-based approaches are not capable of generating BIRs for new scenes not used during training [28] or generating BIRs for standard inputs taken by physics-based BIR simulators [29]. MESH2IR [39] can generate monaural IRs from 3D mesh models. Therefore, we compare the acoustic metrics of MESH2IR separately with the left and right channels and report the average error. We highlight the accuracy improvements in Table 4. We can see that our Listen2Scene outperforms MESH2IR and other variants of the

Table 2: The binaural impulse responses (BIR) synthesized for real-world 3D scenes. We compare the accuracy of our learning-based sound propagation method (Listen2Scene) with geometric sound propagation algorithms. These 3D reconstructed scenes were not used in the training data for Listen2Scene. Our Listen2Scene can synthesize BIRs corresponding to left and right channels by considering interaural level differences (ILD) and interaural time differences (ITD). We can see high-level structures of BIRs from our Listen2Scene is similar to the geometric-based method. The mean absolute error of the normalized BIRs (MAE) is less than 0.5×10^{-2} .



Listen2Scene network.

6.3 Time-domain comparison

We plot additional time-domain representation of BIRs generated using a geometric-based sound propagation approach [48] and our proposed Listen2Scene (Table 2) for two different 3D scenes. We can see that the amount of reverberation and the high-level structures of the BIRs generated using our approach match BIRs generated using the geometric-based method. Also, we can see that the ILD and ITD in our generated BIRs match the BIRs from a geometric method. The mean absolute error of the normalized BIRs generated using Listen2Scene is less than 0.5×10^{-2} .

6.4 Run time

We generated 2500 BIRs for a given 3D scene to calculate the run time. Our network comprises a graph neural network (GNN) and a BIR generator network. For a given 3D scene, we perform mesh encoding using GNN only once, and we generate BIRs by varying source and listener positions. On average, our network takes 0.21 seconds to encode the scene using GNN and 0.023 milliseconds to generate a BIR. Therefore, on average, our network takes 0.1 milliseconds per BIR to generate 2500 BIRs for a given 3D scene. On average, interactive image-based geometric sound propagation

algorithm [2] takes around 0.15 seconds to generate an impulse response [42]. Therefore, our Listen2Scene is more than two orders of magnitude faster than image-based sound propagation methods [2].

7 PERCEPTUAL EVALUATION

We perceptually evaluate the audio rendered using Listen2Scene and compare them with prior learning-based and geometric-based sound propagation algorithms. Our study aims to verify whether the audio rendered using our Listen2Scene is plausible (with left and right channels). We auralized three scenes with a single sound source and two scenes with two sound sources from the ScanNet test dataset (more details in the video). Fig. 1 shows the snapshot of 5 scenes used to evaluate the quality of our proposed audio rendering method. We created a 40-second video of each scene by moving the listener around the scene. Fig. 9 shows the listener path in a 3D scene with two sound sources. We evaluate our approach by adding sounds synthesized using different methods to the 3D scene walkthrough: clean or dry sound (Clean), sound propagation effects created using MESH2IR, Listen2Scene-No-Material, geometric-based method and Listen2Scene. We also compared the reverberant speech created using Listen2Scene-No-Material and Listen2Scene with the captured / real-world IRs from two different scenes in the BRAS dataset (Fig. 8).

Table 3: The responses from the acoustic experts and AMT participants on the plausibility of the sounds in each video created using 3D scenes in the ScanNet. We report the response from each age-category separately and the standard deviation (SD) of the combined results. We shifted our rating scale from -2 - 2 to 1 - 5 and calculated the SD (§ 7.3). We compare video auralized using our Listen2Scene approach with the videos auralized using clean speech, MESH2IR, Listen2Scene-No-Mat and geometric-method. We compare Listen2Scene-No-Mat using a single source in medium (M) and large (L) 3D scenes. We observe that 67% of total participants prefer Listen2Scene when we play video generated using Listen2Scene and MESH2IR with a single source. The highest comparative percentage is **bolded**.

Participants		Acoustic Experts (13 participants) [%]			AMT (57 participants) [%]			Combined (70 participants) [%]			
Baseline Method	No of Sources	Baseline	No Preference	Listen2Scene	Baseline	No Preference	Listen2Scene	Baseline	No Preference	Listen2Scene	SD
Clean	1	15.38	0.00	84.62	29.82	1.76	68.42	27.14	1.43	71.43	1.44
	2	7.69	0.00	92.31	19.30	3.51	77.19	17.14	2.86	80	1.39
Mesh2IR [39]	1	23.08	0.00	76.92	31.58	3.51	64.91	30	2.86	67.14	1.51
	2	15.38	7.69	76.92	15.79	5.26	78.95	15.71	5.71	78.57	1.26
Listen2Scene-No-Mat	1 (M)	30.77	23.08	46.15	29.82	19.30	50.88	30	20	50	1.29
	1 (L)	7.69	30.77	61.54	26.31	7.02	66.66	22.85	11.43	65.71	1.15
	2	23.08	23.08	53.85	22.81	15.79	61.40	22.86	17.14	60	1.30
Geometric-Method	2	23.08	46.15	30.77	38.60	12.28	49.12	35.71	18.57	45.71	1.43
Age Category		18 - 24 (16 participants) [%]			25 - 34 (47 participants) [%]			35 or older (7 participants) [%]			
Baseline Method	No of Sources	Baseline	No Preference	Listen2Scene	Baseline	No Preference	Listen2Scene	Baseline	No Preference	Listen2Scene	SD
Clean	1	31.25	0.00	68.75	19.15	2.13	78.72	71.43	0.00	25.57	
	2	12.5	0.00	87.5	14.89	2.13	82.98	42.86	14.28	42.86	
Mesh2IR [39]	1	18.75	6.25	75.00	34.04	0.00	65.96	28.57	14.28	57.14	
	2	12.5	6.25	81.25	14.89	4.26	80.85	28.57	14.28	57.14	
Listen2Scene-No-Mat	1 (M)	18.75	0.00	81.25	36.17	25.53	38.30	14.28	28.57	57.14	
	1 (L)	12.5	12.5	75.00	21.28	12.77	65.96	57.14	0.00	42.86	
	2	6.25	18.75	75.00	27.66	17.02	55.32	28.57	14.29	57.14	
Geometric-Method	1 (L)	31.25	25.00	43.75	27.66	23.40	48.94	42.86	14.23	42.86	

Table 4: We calculate the mean absolute reverberation time (T_{60}) error, direct-to-reverberant ratio (DRR) error and early-decay-time (EDT) error for monaural IRs generated using MESH2IR and BIRs generated using our approach with materials (Listen2Scene) and without material (Listen2Scene-No-Mat), Listen2Scene-Full, Listen2Scene-No-BIR, and Listen2Scene-ED. We compare them with BIRs computed using the geometric method (§ 3.1). We compare the monaural IRs generated using MESH2IR with each channel in BIRs separately and compute the average. The best results of each metric are shown in **bold**.

IR Dataset	Mean Absolute Error ↓		
	T_{60} (s)	DRR (dB)	EDT (s)
MESH2IR [39]	0.16	5.06	0.25
Listen2Scene-No-Mat	0.10	3.15	0.14
Listen2Scene-Full	0.10	3.18	0.16
Listen2Scene-Fix	0.11	2.56	0.17
Listen2Scene-No-BIR	0.08	4.21	0.21
Listen2Scene-ED	0.10	3.49	0.16
Listen2Scene	0.08	1.7	0.13

Table 5: The total participants’ (acoustic experts and AMT participants) responses on which synthetic speech sample is closer to real-world speech created using captured IRs in the BRAS dataset. We created synthetic speech samples using Listen2Scene and Listen2Scene-No-Material for 2 different real-world environments. The highest comparative percentage is **bolded**.

Environment	Listen2Scene-No-Material	Listen2Scene
Chamber music hall	44.29%	55.71%
Auditorium	21.43%	78.57%

7.1 Participants

We conducted our user study among the acoustic experts (13 participants) and the participants from Amazon Mechanical Turk (AMT) (57 participants), an online crowdsourcing platform that can be used

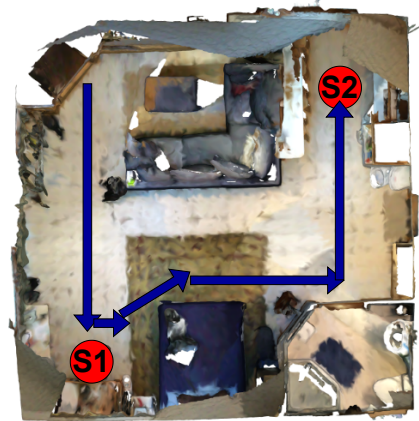


Figure 9: The path covered by the listener in a real-world 3D scene (studio apartment) with two sound sources. The listener path is shown in blue arrows. The red circle represent the two sound sources in the 3D scene. The source S1 is a speech signal from a speaker, and the source S2 is water pouring from the kitchen.

to collect data from diverse participants. Since we have a limited number of acoustic experts to evaluate our approach, we also evaluated using AMT. We conducted our user study on 70 participants (47 males and 23 females), of which 16 participants were between 18 and 24 years of age, 48 participants were between 25 and 34 years of age, and 7 participants were above 35 years of age. We ensured the quality of our evaluation by pre-screening the participants. As our pre-screening questions, we asked the online participants whether they use headphones with a laptop/desktop and only allowed them to proceed with the survey if they answered yes. The average completion time of our user study is 20 minutes for each user. The just-noticeable-difference (JND) relative reverberation time change is 5% - 25% [4]. On average on each rendered 40-second video,

the reverberation time changes by 30%. Therefore, under normal conditions, we expect the listeners to identify the relative changes in the audio correctly.

7.2 Benchmarks

We performed the following five benchmark comparisons in perceptual evaluation. Our first four benchmarks compare 40-second-long audio-rendered 3D environment walkthrough videos from our Listen2Scene with baseline methods. In our last benchmark, we compare the real speech with speech rendered using our Listen2Scene and Listen2Scene-No-Material.

Clean vs. Listen2Scene: We compared audio-rendered 3D scenes with and without acoustic effects from Listen2Scene. We created two different 3D scene walkthrough videos for our experiment with a single sound source and two sound sources. For a single sound source, we evaluate whether our approach creates continuous and smooth acoustic effects when moving around the scene and whether the user can perceive the indirect acoustic effects. In the two sound sources walkthrough video, we evaluate whether the relative distance between the two sound sources in the rendered audio using our Listen2Scene matches the video.

MESH2IR vs. Listen2Scene: We auralized a 3D walkthrough video each for a single source and two sources. We use the prior monaural audio rendering method MESH2IR and our proposed binaural audio rendering approach, Listen2Scene, for our comparison. We aim to investigate whether the participants feel that the acoustic effects in the left and right ears change smoothly and synchronously as the user walks into the real-world 3D scene. In addition to distance, we investigate whether our acoustic effects change smoothly with the direction of the source. We also evaluated whether our approach is plausible even when there is more than one source in the 3D scene.

Listen2Scene-No-Material vs. Listen2Scene: We auralized two real-world 3D scenes with a single source from a medium-sized and a large 3D scene, and another 3D scene with two sources. In this experiment, we evaluate whether the reverberation effects from Listen2Scene match closely with the environment when compared with Listen2Scene-No-Material. Our goal is to evaluate the perceptual benefits of adding material characteristics to our learning method. The amount of reverberation varies with the size of the 3D scene, therefore we compare the contribution of material to the plausibility of auralized medium and large 3D scenes. In real environments, the listener hears audio from multiple sound sources. Therefore, we evaluate the plausibility of our approach when more than one source is played in the 3D walkthrough video.

Geometric-method vs. Listen2Scene: We auralized one real-world 3D scene with two sources. In this experiment, we evaluate whether the participants feel the Listen2Scene or the geometric-based sound propagation [48] is more plausible for the corresponding 3D scene walkthrough video.

BRAS benchmark: We played reverberant speech created using captured left channel IRs from the BRAS and left channel impulse responses synthesized using our Listen2Scene and Listen2Scene-No-Material in two different 3D scenes (Fig. 8). We use single-channel IRs to remove acoustic effects from ITD and ILD and make the participants focus on reverberation effects corresponding to the complexity and shape of the environment. We asked the participants to choose which speech sampled auralized using our BIRs is closer to the real speech from the BRAS.

7.3 Experiment and Results

In our experiment, we randomly choose the location of two videos (left or right) used for the comparison to eliminate bias from collected data and ask the participants to rate from -2 to +2 based on which video sounds more plausible, i.e. the way the sound varies

in both ears when the listener moves towards and away from the sound source. The participants rate -2 if the left video sounds more plausible and vice versa. If the participants have no preference, they rate 0. We group the negative scores (-1 and -2) and positive scores (1 and 2) to choose the participants' preferences.

Table 3 summarises all the participants' responses. We observe that 67% - 79% of the total participants find that the auralized scenes with 1-2 sources using Listen2Scene are more plausible than MESH2IR. Interestingly, 17% - 27% of total participants find that just adding clean sound to a 3D scene video is more plausible. When we further break down our results based on age, we observe that 42.86% to 71.43% of 35 or older participants prefer adding just clean sound to the video. We believe that this might be caused by an increase in volume from our approach when the listener moves too close to the speaker. All of our participants older than 35 are from AMT, therefore we were not able to get feedback from the participants after the studies. We also observed that when there is more than one source in the 3D scene, the relative sound variation of the sources based on their location is more plausible with Listen2Scene, as compared to using dry sound or MESH2IR. In large 3D models, where the T_{60} tends to be higher, 66% of participants feel Listen2Scene is more plausible than Listen2Scene-No-Material. We also can see that 10% more participants feel our learning-based approach is more plausible than the geometric-based method. The BIRs generated using the learning-based method smoothly change with the distance and listeners can feel a smooth transition in audio when they move to different positions in the 3D scene. From Table 5, we can see that audio/speech rendered using our Listen2Scene approach is closer to the real-world speech. Overall, we notice that our approach creates plausible acoustic effects when there are one or more sound sources in the 3D scene.

8 CONCLUSION LIMITATIONS AND FUTURE WORK

We present a material-aware learning-based sound propagation approach to render thousands of audio samples on the fly for a given real 3D scene. We propose a novel approach to handle material properties in our network. Moreover, we show that adding material information significantly improves the accuracy of BIR generation using our Listen2Scene approach and is comparable to geometric propagation methods or captured BIRs in terms of acoustic characteristics and perceptual evaluation. Overall, our algorithm offers two orders of magnitude performance improvement over interactive geometric sound propagation methods.

Our approach has some limitations. The performance of our network depends on the training data. We can train our network with real captured BIRs, though it is challenging and expensive to capture a large number of such BIRs. Currently, we use BIRs generated using geometric algorithms for medium-sized 3D scenes in the ScanNet dataset for training, and the overall accuracy of Listen2Scene is also a function of the accuracy of the training data. Our approach is limited to static real scenes. Our material classification methods assume that accurate semantic labels for each object in the scene are known. It is possible to consider sub-band acoustic material coefficients to further improve the accuracy. However, the complexity of the graph representation of the 3D scene drastically increases, and we are limited by the GPU memory in handling such complex graphs. Due to the limitation of the training dataset used for training, the performance of our network has been currently evaluated on small and medium-sized scenes. In future work, we like to train and evaluate our approach on very large scenes. Since the ScanNet dataset does not have the same 3D environment with different structural changes, we are not able to train and evaluate different structural detail resolutions. As part of future work, it would be useful to analyze our learning-based sound propagation approach on different structural detail resolutions.

REFERENCES

- [1] A. Allen and N. Raghuvanshi. Aerophones in flatland: interactive wave simulation of wind instruments. *ACM Trans. Graph.*, 34(4):134:1–134:11, 2015.
- [2] J. B. Allen and D. A. Berkley. Image method for efficiently simulating small-room acoustics. *The Journal of the Acoustical Society of America*, 65(4):943–950, 04 1979. doi: 10.1121/1.382599
- [3] L. Aspöck, M. Vorländer, F. Brinkmann, D. Ackermann, and S. Weinzierl. Benchmark for room acoustical simulation (bras). *DOI*, 10:14279, 2020.
- [4] M. G. Blevins, A. T. Buck, Z. Peng, and L. M. Wang. Quantifying the just noticeable difference of reverberation time with band-limited noise centered around 1000 hz using a transformed up-down adaptive method. In *International Symposium on Room Acoustics*, 2013.
- [5] F. Brinkmann, L. Aspöck, D. Ackermann, S. Lepa, M. Vorländer, and S. Weinzierl. A round robin on room acoustical simulation and auralization. *The Journal of the Acoustical Society of America*, 145(4):2746–2760, 2019.
- [6] C. Chen, C. Schissler, S. Garg, P. Kobernik, A. Clegg, P. Calamia, D. Batra, P. W. Robinson, and K. Grauman. Soundspaces 2.0: A simulation platform for visual-acoustic learning. *arXiv preprint arXiv:2206.08312*, 2022.
- [7] A. Dai, A. X. Chang, M. Savva, M. Halber, T. A. Funkhouser, and M. Nießner. Scannet: Richly-annotated 3d reconstructions of indoor scenes. In *CVPR*, pp. 2432–2443. IEEE Computer Society, 2017.
- [8] A. Dai, M. Nießner, M. Zollhöfer, S. Izadi, and C. Theobalt. Bundlefusion: Real-time globally consistent 3d reconstruction using on-the-fly surface reintegration. *ACM Trans. Graph.*, 36(4), jul 2017. doi: 10.1145/3072959.3054739
- [9] Dawson-Haggerty et al. trimesh.
- [10] J. Eaton, N. D. Gaubitch, A. H. Moore, and P. A. Naylor. Estimation of room acoustic parameters: The ace challenge. *IEEE/ACM Transactions on Audio, Speech, and Language Processing*, 24(10):1681–1693, 2016. doi: 10.1109/TASLP.2016.2577502
- [11] H. Gao and S. Ji. Graph u-nets. In *ICML*, vol. 97 of *Proceedings of Machine Learning Research*, pp. 2083–2092. PMLR, 2019.
- [12] J. Gauthier. Conditional generative adversarial networks for convolutional face generation. In *Tech Report*, 2015.
- [13] A. F. Genovese, H. Gamper, V. Pulkki, N. Raghuvanshi, and I. J. Tashev. Blind room volume estimation from single-channel noisy speech. In *ICASSP 2019 - 2019 IEEE International Conference on Acoustics, Speech and Signal Processing (ICASSP)*, pp. 231–235, 2019. doi: 10.1109/ICASSP.2019.8682951
- [14] N. A. Gumerov and R. Duraiswami. A broadband fast multipole accelerated boundary element method for the 3d helmholtz equation. 2008.
- [15] J. Jot. An analysis/synthesis approach to real-time artificial reverberation. In *ICASSP*, pp. 221–224. IEEE Computer Society, 1992.
- [16] T. N. Kipf and M. Welling. Semi-supervised classification with graph convolutional networks. In *ICLR (Poster)*. OpenReview.net, 2017.
- [17] C. Kling. Absorption coefficient database, Jul 2018.
- [18] B. Knyazev, G. W. Taylor, and M. R. Amer. Understanding attention and generalization in graph neural networks. In *NeurIPS*, pp. 4204–4214, 2019.
- [19] H. Kon and H. Koike. Estimation of late reverberation characteristics from a single two-dimensional environmental image using convolutional neural networks. *Journal of the audio engineering society*, 67(7/8):540–548, July 2019. doi: 10.17743/jaes.2018.0069
- [20] H. Kuttruff. Auralization of impulse responses modeled on the basis of ray-tracing results. *Journal of the audio engineering society*, 41(11):876–880, November 1993.
- [21] H. Kuttruff. *Room acoustics*. Crc Press, 2016.
- [22] P. Larsson, D. Vastfjäll, and M. Kleiner. Better presence and performance in virtual environments by improved binaural sound rendering. In *Audio Engineering Society Conference: 22nd International Conference: Virtual, Synthetic, and Entertainment Audio*. Audio Engineering Society, 2002.
- [23] T. Lentz, D. Schröder, M. Vorländer, and I. Assenmacher. Virtual reality system with integrated sound field simulation and reproduction. *EURASIP J. Adv. Signal Process*, 2007(1):187, jan 2007. doi: 10.1155/2007/70540
- [24] D. Li, T. R. Langlois, and C. Zheng. Scene-aware audio for 360° videos. *ACM Trans. Graph.*, 37(4), jul 2018. doi: 10.1145/3197517.3201391
- [25] C. Liu, A. G. Schwing, K. Kundu, R. Urtasun, and S. Fidler. Rent3d: Floor-plan priors for monocular layout estimation. In *CVPR*, pp. 3413–3421. IEEE Computer Society, 2015.
- [26] Q. Liu, M. J. Kusner, and P. Blunsom. A survey on contextual embeddings. *arXiv preprint arXiv:2003.07278*, 2020.
- [27] S. Liu and D. Manocha. Sound synthesis, propagation, and rendering. *Synthesis Lectures on Visual Computing: Computer Graphics, Animation, Computational Photography, and Imaging*, 11(2):1–110, 2022.
- [28] A. Luo, Y. Du, M. J. Tarr, J. B. Tenenbaum, A. Torralba, and C. Gan. Learning neural acoustic fields. *arXiv preprint arXiv:2204.00628*, 2022.
- [29] S. Majumder, C. Chen, Z. Al-Halah, and K. Grauman. Few-shot audio-visual learning of environment acoustics. *arXiv preprint arXiv:2206.04006*, 2022.
- [30] R. Mehra, N. Raghuvanshi, L. Antani, A. Chandak, S. Curtis, and D. Manocha. Wave-based sound propagation in large open scenes using an equivalent source formulation. *ACM Trans. Graph.*, 32(2):19:1–19:13, 2013.
- [31] R. Mehra, A. Rungta, A. Golas, M. Lin, and D. Manocha. Wave: Interactive wave-based sound propagation for virtual environments. *IEEE Transactions on Visualization and Computer Graphics*, 21(4):434–442, 2015. doi: 10.1109/TVCG.2015.2391858
- [32] M. Mirza and S. Osindero. Conditional generative adversarial nets. *arXiv preprint arXiv:1411.1784*, 2014.
- [33] M. K. Mishra and J. Viradiya. Survey of sentence embedding methods. *International Journal of Applied Science and Computations*, 6(3):592–592, 2019.
- [34] A. Muntoni and P. Cignoni. PyMeshLab, Jan. 2021. doi: 10.5281/zenodo.4438750
- [35] P. A. Naylor and N. D. Gaubitch. *Speech Dereverberation*. Springer Publishing Company, Incorporated, 1st ed., 2010.
- [36] N. Raghuvanshi, R. Narain, and M. C. Lin. Efficient and accurate sound propagation using adaptive rectangular decomposition. *IEEE Trans. Vis. Comput. Graph.*, 15(5):789–801, 2009.
- [37] N. Raghuvanshi, J. M. Snyder, R. Mehra, M. C. Lin, and N. K. Govindaraju. Precomputed wave simulation for real-time sound propagation of dynamic sources in complex scenes. *ACM Trans. Graph.*, 29(4):68:1–68:11, 2010.
- [38] A. Ratnarajah, I. Ananthabhotla, V. K. Ithapu, P. Hoffmann, D. Manocha, and P. Calamia. Towards improved room impulse response estimation for speech recognition. *arXiv preprint arXiv:2211.04473*, 2022.
- [39] A. Ratnarajah, Z. Tang, R. Aralikatti, and D. Manocha. MESH2IR: neural acoustic impulse response generator for complex 3d scenes. In *ACM Multimedia*, pp. 924–933. ACM, 2022.
- [40] A. Ratnarajah, Z. Tang, and D. Manocha. IR-GAN: room impulse response generator for far-field speech recognition. In *Interspeech*, pp. 286–290. ISCA, 2021.
- [41] A. Ratnarajah, Z. Tang, and D. Manocha. Ts-rir: Translated synthetic room impulse responses for speech augmentation. In *2021 IEEE Automatic Speech Recognition and Understanding Workshop (ASRU)*, pp. 259–266, 2021. doi: 10.1109/ASRU51503.2021.9688304
- [42] A. Ratnarajah, S. Zhang, M. Yu, Z. Tang, D. Manocha, and D. Yu. Fast-rir: Fast neural diffuse room impulse response generator. In *ICASSP*, pp. 571–575. IEEE, 2022.
- [43] Z. Ren, H. Yeh, and M. C. Lin. Example-guided physically based modal sound synthesis. *ACM Transactions on Graphics (TOG)*, 32(1):1–16, 2013.
- [44] L. Savioja. Real-time 3d finite-difference time-domain simulation of low- and mid-frequency room acoustics. In *13th Int. Conf on Digital Audio Effects*, vol. 1, p. 75, 2010.
- [45] L. Savioja and U. P. Svensson. Overview of geometrical room acoustic modeling techniques. *The Journal of the Acoustical Society of America*, 138(2):708–730, 2015. doi: 10.1121/1.4926438
- [46] C. Schissler, C. Loftin, and D. Manocha. Acoustic classification and

- optimization for multi-modal rendering of real-world scenes. *IEEE transactions on visualization and computer graphics*, 24(3):1246–1259, 2017.
- [47] C. Schissler and D. Manocha. gsound: interactive sound propagation for games. *journal of the audio engineering society*, february 2011.
- [48] C. Schissler and D. Manocha. Interactive sound propagation and rendering for large multi-source scenes. *ACM Trans. Graph.*, 36(1):2:1–2:12, 2017.
- [49] C. Schissler, R. Mehra, and D. Manocha. High-order diffraction and diffuse reflections for interactive sound propagation in large environments. *ACM Trans. Graph.*, 33(4), jul 2014. doi: 10.1145/2601097.2601216
- [50] M. R. Schroeder. New method of measuring reverberation time. *The Journal of the Acoustical Society of America*, 37(6):1187–1188, 1965. doi: 10.1121/1.1939454
- [51] H. S. Seddeq. Factors influencing acoustic performance of sound absorptive materials. *Australian journal of basic and applied sciences*, 3(4):4610–4617, 2009.
- [52] N. Singh, J. Mentch, J. Ng, M. Beveridge, and I. Drori. Image2reverberb: Cross-modal reverber impulse response synthesis. In *ICCV*, pp. 286–295. IEEE, 2021.
- [53] C. J. Steinmetz, V. K. Ithapu, and P. Calamia. Filtered noise shaping for time domain room impulse response estimation from reverberant speech. In *2021 IEEE Workshop on Applications of Signal Processing to Audio and Acoustics (WASPAA)*, pp. 221–225, 2021. doi: 10.1109/WASPAA52581.2021.9632680
- [54] K. Su, M. Chen, and E. Shlizerman. INRAS: Implicit neural representation for audio scenes. In A. H. Oh, A. Agarwal, D. Belgrave, and K. Cho, eds., *Advances in Neural Information Processing Systems*, 2022.
- [55] P. Tang, S. Vick, J. Chen, and S. German Paal. Chapter 2 - surveying, geomatics, and 3d reconstruction. In I. Brilakis and C. Haas, eds., *Infrastructure Computer Vision*, pp. 13–64. Butterworth-Heinemann, 2020. doi: 10.1016/B978-0-12-815503-5.00002-4
- [56] Z. Tang, R. Aralikatti, A. J. Ratnarajah, and D. Manocha. GWA: A large high-quality acoustic dataset for audio processing. In *SIGGRAPH (Conference Paper Track)*, pp. 36:1–36:9. ACM, 2022.
- [57] Z. Tang, N. J. Bryan, D. Li, T. R. Langlois, and D. Manocha. Scene-aware audio rendering via deep acoustic analysis. *IEEE transactions on visualization and computer graphics*, 26(5):1991–2001, 2020.
- [58] Z. Tang, L. Chen, B. Wu, D. Yu, and D. Manocha. Improving reverberant speech training using diffuse acoustic simulation. In *ICASSP 2020 - 2020 IEEE International Conference on Acoustics, Speech and Signal Processing (ICASSP)*, pp. 6969–6973, 2020.
- [59] Z. Tang, H.-Y. Meng, and D. Manocha. Learning acoustic scattering fields for dynamic interactive sound propagation. In *2021 IEEE Virtual Reality and 3D User Interfaces (VR)*, pp. 835–844, 2021. doi: 10.1109/VR50410.2021.00111
- [60] L. L. Thompson. A review of finite-element methods for time-harmonic acoustics. *The Journal of the Acoustical Society of America*, 119(3):1315–1330, 2006. doi: 10.1121/1.2164987
- [61] R. Wang and D. Manocha. Dynamic coherence-based em ray tracing simulations in vehicular environments. In *2022 IEEE 95th Vehicular Technology Conference: (VTC2022-Spring)*, pp. 1–7, 2022. doi: 10.1109/VTC2022-Spring54318.2022.9860362
- [62] F. L. Wightman and D. J. Kistler. The dominant role of low-frequency interaural time differences in sound localization. *The Journal of the Acoustical Society of America*, 91 3:1648–61, 1992.
- [63] C. Yeshwanth, Y.-C. Liu, M. Nießner, and A. Dai. Scannet++: A high-fidelity dataset of 3d indoor scenes. In *Proceedings of the International Conference on Computer Vision (ICCV)*, 2023.